LUND UNIVERSITY

A quantitative pixel-wise measurement of myocardial blood flow by contrast-enhanced first-pass CMR perfusion imaging: microsphere validation in dogs and feasibility study in humans.

Hsu, L-Y; Groves, D W; Aletras, Anthony; Kellman, P; Arai, A E

Link to publication

A Quantitative Pixel-Wise Measurement of Myocardial Blood Flow by Contrast-Enhanced First-Pass CMR Perfusion Imaging

Microsphere Validation in Dogs and Feasibility Study in Humans

Li-Yueh Hsu, DSc, Daniel W. Groves, MD, Anthony H. Aletras, PhD, Peter Kellman, PhD,
Andrew E. Arai, MD

Bethesda, Maryland

OBJECTIVES The aim of this study was to evaluate fully quantitative myocardial blood flow (MBF) at a pixel level based on contrast-enhanced first-pass cardiac magnetic resonance (CMR) imaging in dogs and in patients.

BACKGROUND Microspheres can quantify MBF in subgram regions of interest, but CMR perfusion imaging may be able to quantify MBF and differentiate blood flow at a much higher resolution.

METHODS First-pass CMR perfusion imaging was performed in a dog model with local hyperemia induced by intracoronary adenosine. Fluorescent microspheres were the reference standard for MBF validation. CMR perfusion imaging was also performed on patients with significant coronary artery disease (CAD) by invasive coronary angiography. Myocardial time-signal intensity curves of the images were quantified on a pixel-by-pixel basis using a model-constrained deconvolution analysis.

RESULTS Qualitatively, color CMR perfusion pixel maps were comparable to microsphere MBF bull's-eye plots in all animals. Pixel-wise CMR MBF estimates correlated well against subgram (0.49 ± 0.14 g) microsphere measurements ($r = 0.87$ to 0.90) but showed minor underestimation of MBF. To reduce bias due to misregistration and minimize issues related to repeated measures, 1 hyperemic and 1 remote sector per animal were compared with the microsphere MBF, which improved the correlation ($r = 0.97$ to 0.98), and the bias was close to zero. Sector-wise and pixel-wise CMR MBF estimates also correlated well ($r = 0.97$). In patients, color CMR stress perfusion pixel maps showed regional blood flow decreases and transmural perfusion gradients in territories served by stenotic coronary arteries. MBF estimates in endocardial versus epicardial subsectors, and ischemic versus remote sectors, were all significantly different ($p < 0.001$ and $p < 0.01$, respectively).

CONCLUSIONS Myocardial blood flow can be quantified at the pixel level ($\sim$32 μl of myocardium) on CMR perfusion images, and results compared well with microsphere measurements. High-resolution pixel-wise CMR perfusion maps can quantify transmural perfusion gradients in patients with CAD. (J Am Coll Cardiol Img 2012;5:154–66) © 2012 by the American College of Cardiology Foundation

First-pass gadolinium-enhanced cardiac magnetic resonance (CMR) perfusion imaging is effective in detecting and diagnosing coronary artery disease (CAD) in patients (1–11). Several studies have used semiquantitative approaches to measure first-pass CMR perfusion images. Although these methods are generally simple, semiquantitative perfusion estimates compress the effects of vasodilation into a narrower range of perfusion values compared with fully quantitative estimates (12,13). Myocardial blood flow (MBF) can be estimated from first-pass CMR perfusion

images (12,14–18). These validation studies showed that fully quantitative MBF estimates from CMR correlated well with absolute MBF as measured by microspheres. However, these studies were performed on a sector-by-sector basis to improve signal-to-noise ratio and to mitigate motion artifacts. This approach inherently downgrades the resolution of CMR perfusion information to significantly larger regions of interest.

The aim of this study was to evaluate whether first-pass CMR perfusion imaging has sufficient spatial resolution to estimate fully quantitative MBF at the pixel level. We developed a computer-based method for pixel-wise MBF quantification from CMR perfusion images. The results of the fully quantitative pixel-wise CMR MBF estimates were compared with absolute MBF as determined by microsphere measurements in canines. The heterogeneity of pixel-wise CMR perfusion MBF estimates was studied within myocardial sectors. To evaluate the feasibility of this method in a clinically relevant model, pixel-wise CMR perfusion maps were examined in patients with significant coronary stenosis as determined by invasive coronary angiography to determine whether endocardial to epicardial perfusion gradients could be detected.

METHODS

Experimental preparation. The study protocol was reviewed and approved by the Animal Care and Use Committee of the National Heart, Lung, and Blood Institute (NHLBI). Seven healthy mongrel dogs weighing between 10 and 22 kg were used in this study. The animals were anesthetized with 1% to 2% isoflurane during the experiment. Instrumentation of each animal included 2 femoral arterial lines for blood pressure monitoring and microsphere blood sample withdrawals, a left atrial catheter for microsphere injection, and a catheter in a right ventricular branch of the left anterior descending coronary artery (LAD) for a local adenosine infusion.

Approximately 5 million 15-μm fluorescence-labeled microspheres (Interactive Medical Technologies, Irvine, California) were administered during reference blood sampling (10 ml/min for 3 min) to measure absolute MBF (in ml/min/g) at baseline and during adenosine infusion. Adenosine was infused at 20 μg/kg/min and diluted with normal saline to provide an intracoronary injection rate of 1 ml/min to produce a local hyperemic zone. Microspheres and CMR perfusion imaging was performed within 5 to 10 min during the same adenosine infusion.

CMR perfusion imaging. The CMR perfusion images were acquired with a 1.5-T scanner (Magnetom Avanto, Siemens Healthcare, Erlangen, Germany) using a steady-state free precession sequence with saturation recovery magnetization preparation (19). A dual-bolus technique (12) was used that consisted of 2 doses of gadolinium diethylenetriamine pentaacetic acid (DTPA) (Magnevist; Berlex Laboratories, Wayne, New Jersey) at 0.005 mmol/kg and 0.05 mmol/kg diluted into equal volumes and injected at 2 ml/s followed by a 20-ml saline flush. Two or 3 short-axis images were collected every R-R interval for 60 heartbeats for each bolus during a breath-hold by transiently stopping a mechanical ventilator.

Typical imaging parameters included a 90° composite saturation preparation pulse, 50° readout pulse, saturation recovery time = 90 ms, repetition time = 2.6 ms, echo time = 1.3 ms, field of view = 260 × 179 mm, acquisition matrix = 128 × 80, image matrix = 256 × 176 after interpolation, slice thickness = 7 mm. Each voxel represents approximately 32 μl of myocardium (or 33 mg/voxel). Parallel imaging with an acceleration factor of 2 was used. Two proton density–weighted images were also acquired to allow correction of surface coil B$_1$-field inhomogeneity.

Microsphere processing. After perfusion imaging, the animals were euthanized with potassium chloride while under anesthesia. The heart was removed and placed in agar to facilitate cutting into 3.5-mm short-axis slices. The papillary muscles and right ventricular walls were excluded before microsphere processing. A pair of adjacent pathological slices was matched to a 7-mm short-axis CMR perfusion image based on anatomic landmarks. The pair of

the pathological slices was divided into 8 circumferential sectors that were further subdivided into epicardial and endocardial sectors (16 sectors per slice). Tissue samples and blood reference samples were processed to provide microsphere measurements of MBF (ml/min/g) per specimen.

Clinical CMR protocol. The clinical study protocol was reviewed and approved by the institutional review board of the NHLBI, and all participants gave written informed consent. Dipyridamole stress (0.56 mg/kg) and rest CMR perfusion imaging were performed on a healthy volunteer and 5 patients (4 men and 1 woman, mean age 59 ± 12 years) with known or suspected CAD. All patients had coronary artery stenosis confirmed by coronary catheterization within 60 days of the CMR. The CMR imaging was performed using a steady-state free precession, dual-sequence method (20) with imaging parameters similar to the animal study. This dual-sequence method obtains a low-resolution arterial input function image and 3 myocardial images during each R-R interval. A gadolinium DTPA contrast at 0.05 mmol/kg was injected at 5 ml/s during the first-pass perfusion imaging.

Sector-wise CMR perfusion image analysis. To compare sector-wise MBF measurements from CMR perfusion images and microsphere MBF, endocardial and epicardial borders of the left ventricular (LV) myocardium were manually traced on a perfusion image series using Argus CMR software (Syngo, Siemens Healthcare). The myocardial region of interest defined by these borders was divided into 8 circumferential sectors, and then subdivided into epicardial and endocardial sectors to match the corresponding 16 sectors of the pathological slice in all animals.

Myocardial time-signal intensity curves were generated from the myocardial region of interest of the perfusion image series. The arterial input function was measured from the low-dose contrast or low-resolution image series. B_1 normalized time-signal intensity curves were quantified using a model-constrained deconvolution (as explained in a later section) to obtain sector-wise MBF estimates.
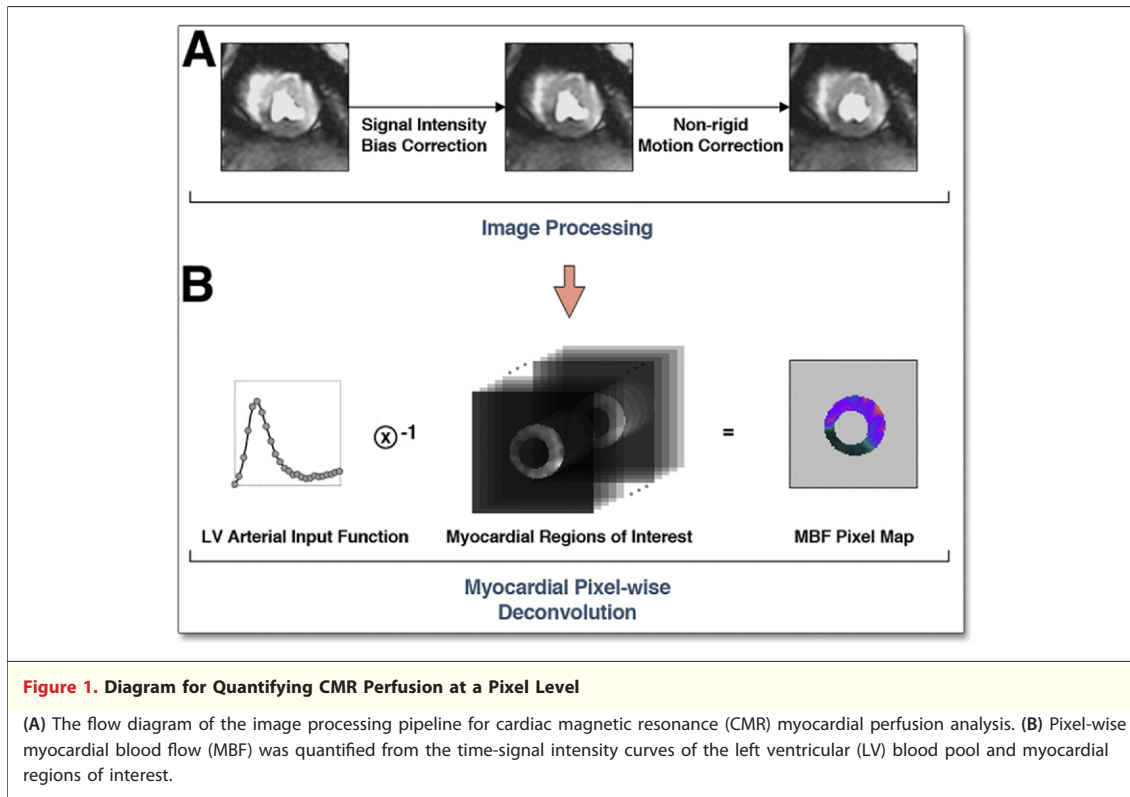
Pixel-wise CMR perfusion image analysis. To compute pixel-wise MBF from CMR perfusion images, a series of image processing steps were performed using custom software developed in Interactive Data Language (ITT Visual Information Solutions, Boulder, Colorado) to obtain the time-signal intensity curve of each pixel in the myocardial regions of interest (Fig. 1). First, B_1-field inhomogeneity was approximated by using a high-order polynomial surface fit with a hierarchical weighting scheme to the proton density–weighted image (21). The estimated signal intensity bias field was then applied to the T_1-weighted perfusion image series to correct for the B_1 inhomogeneity.

Next, rigid and nonrigid image registration methods were performed on the CMR perfusion images to ensure proper propagation of time-signal intensity of the myocardial pixels. All images of the same slice were first registered to the center of the myocardial regions of interest to compensate for rigid-body translational motion. A user-selected landmark at the anterior right ventricular and LV junction line was then used to adjust rigid-body rotational motion. Finally, a nonrigid image registration algorithm was used to correct geometric deformation of the myocardium. This was based on mapping endocardial and epicardial borders of the perfusion image series to 2 common concentric circles that define a new region of interest. The size of the 2 concentric circles was calculated by using average radii of the endocardial and epicardial borders from all images. A closest distance measure was used to obtain the correspondence of control points between myocardial borders and the concentric circles. The myocardial region of interest in each image was then processed by a thin-plate spline warping to compensate for possible deformation of the myocardium.

These image processing steps were used to improve the spatial consistency of the image pixels in the myocardium and to extract pixel-wise myocardial time-signal intensity curves. Pixel-wise time-signal intensity curves were quantified using a model-constrained deconvolution to obtain MBF pixel maps.

MBF quantification. The central volume principle described by Zierler (22,23) in indicator-dilution methods was the basis for MBF quantification. It assumes the system response of contrast transport within a tissue to be linear and stationary. The contrast concentration curve of the tissue can then be expressed as a convolution of the arterial input function and an impulse response function. The impulse response function is a probability density function that characterizes contrast transit times through the system. This function, $h(t)$, can be obtained through a reverse process of deconvolution. Since deconvolution is sensitive to noise, the shape of $h(t)$ is constrained to a mathematical model. The best parameters describing the model are determined by iterative calculations. This overall process is called model-constrained deconvolution (15,24).

Figure 1. Diagram for Quantifying CMR Perfusion at a Pixel Level

(A) The flow diagram of the image processing pipeline for cardiac magnetic resonance (CMR) myocardial perfusion analysis. **(B)** Pixel-wise myocardial blood flow (MBF) was quantified from the time-signal intensity curves of the left ventricular (LV) blood pool and myocardial regions of interest.

Here, we propose a logistic impulse response function, $h(t) = F/(1 + \exp(-(t - \tau) \times k)) + I$, where F represents the magnitude of the function, t and k describe the temporal delay length and decay rate, respectively, of $h(t)$ due to dynamically changing contrast concentration. This model differs from the commonly used Fermi function (15,25) by the introduction of an interstitial offset term I. This parameter provides a linear shift of the impulse response function from zero during and after the first pass, which accounts for leakage of the contrast into the interstitial space and the slow clearance relative to the first-pass kinetics. MBF in both pixel-wise and sector-wise analyses was estimated using this model from the LV arterial input and myocardial time-signal intensity curves.

Statistical analysis. Data are expressed as mean ± SD unless specified. The relationship between CMR estimates of MBF and microsphere reference absolute MBF was evaluated by linear correlation. Limits of agreement were assessed by Bland-Altman plots. Coefficient of variation (CV) was defined as the ratio of the SD to the mean. A p value <0.05 was considered statistically significant.

CMR MBF pixel maps of all animals were divided and then averaged to 8 endocardial and 8 epicardial subsectors to compare with microspheres.

Additionally, subsector averages of MBF pixel maps were also compared with MBF estimates from sector-wise time-signal intensity curves.

In CMR perfusion pixel maps of patients with CAD, endocardial MBF, epicardial MBF, and endocardial-to-epicardial MBF ratios were measured with regions of interest in remote myocardium, and in myocardium served by coronary arteries with significant coronary stenoses. MBF and MBF ratios were compared using a paired Student t test.

RESULTS

Physiological measurements remained reasonably stable during the experiment. The average heart rate was 101 ± 18 beats/min and 98 ± 19 beats/min before and during adenosine infusion, respectively. The average systolic and diastolic blood pressures were 115 ± 11 mm Hg and 68 ± 10 mm Hg, respectively, before the adenosine infusion. Both systolic and diastolic blood pressures dropped slightly to 112 ± 14 mm Hg and 61 ± 8 mm Hg, respectively, during the adenosine infusion. For microsphere processing, the endocardial sectors weighed 0.41 ± 0.09 g (n = 56), epicardial sectors weighed 0.58 ± 0.13 g (n = 56), and transmural sectors averaged 0.99 ± 0.20 g (n = 56). The

median microsphere count in endocardial sectors was 2,974 (range: 926 to 9,569) and in epicardial sectors was 4,677 (range: 1,318 to 15,811). Microsphere results showed successful vasodilation for all canines, defined as at least a 2-fold higher microsphere MBF in hyperemic sectors relative to remote sectors.

Figure 2 compares pixel-wise time-signal intensity curves for hyperemic versus remote regions. A similar time course of contrast enhancement was observed between pixels within the same region. There was a hyperemic response on the adenosine-affected regions as shown by faster contrast wash-in and wash-out kinetics, and a higher overshoot in the pixel-wise time-signal intensity curves.

For qualitative comparisons, Figure 3 shows colorized CMR perfusion pixel maps of all animals with corresponding microsphere MBF on the same absolute color scale. Regional differential blood flow was clearly seen in all animals. Qualitatively, the dynamic range of color perfusion maps from CMR was comparable to microsphere bull's-eye plots in all animals. At the same time, there were also sectors that did not correspond perfectly due to spatial misregistration between the CMR imaging slice versus pathological microsphere slice. Nevertheless, CMR perfusion pixel maps had a higher

spatial resolution (0.033 g/voxel) than sector-wise microsphere maps (0.49 g/sector).

For quantitative comparisons, Figure 4 shows pixel-wise CMR MBF estimates averaged into sector-wise measures that correlate well with microsphere MBF in transmural, endocardial, and epicardial sectors (n = 56; r = 0.90, r = 0.89, and r = 0.87, respectively). However, Bland-Altman analysis shows there is a small bias, suggesting CMR underestimates microsphere MBF, or spatial misregistration adds systematic errors to the comparisons.

To reduce the probability of misregistration, further comparisons were performed by selecting 1 hyperemic and 1 remote sector from the center of each zone on both CMR perfusion images and the pathological slice for each animal. There were even tighter correlations between CMR estimates of MBF and microsphere measurements in transmural, endocardial, and epicardial sectors (n = 14; r = 0.98, r = 0.97, and r = 0.97, respectively) (Figure 5). Bland-Altman analysis also showed minimal residual bias for these comparisons.

To address whether quantification of CMR time-signal intensity curves at a pixel level introduces biases relative to quantification of sector-wise time-signal intensity curves, additional correlation and Bland-Altman analysis were performed (Fig. 6). There was a strong correlation in transmural, endocardial, and epicardial comparisons (r = 0.97 for all comparisons). Similarly, there was no significant bias in all Bland-Altman plots. This indicates that MBF quantified at the pixel level does not intrinsically alter the perfusion information content of the CMR images as estimated from conventional sector-wise analysis.

To analyze transmural perfusion gradients in our animal model, endocardial MBF, epicardial MBF, and endocardial-to-epicardial MBF ratio were measured on CMR perfusion pixel maps and microspheres. For both hyperemic and remote regions, there were no significant blood flow differences between endocardial and epicardial MBF by CMR or microspheres measurements (Table 1) (all p = NS). When comparing CMR and microspheres MBF measurements, there were also no significant differences between the 2 methods for endocardial hyperemic MBF, epicardial hyperemic MBF, or corresponding measurements in the remote region (Table 1) (all p = NS). However, CMR perfusion pixel maps and microspheres both detected significant differences in MBF between hyperemic and remote regions (Table 1) (all p < 0.01).
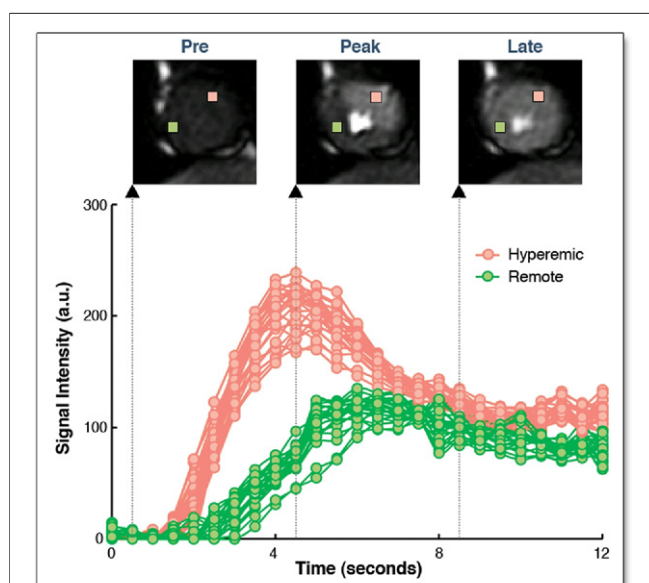
Figure 2. CMR Time-Signal Intensity Curves at a Pixel Level

Pixel-wise myocardial time-signal intensity curves show hyperemic response in an adenosine-induced region (25 pixels in **pink**) compared with a remote region (25 pixels in **green**). A similar time course of contrast enhancement was observed between neighboring pixels within the same region. Example perfusion images at different time points are shown at pre-, peak-, and late contrast enhancement. a.u. = arbitrary units; CMR = cardiac magnetic resonance.
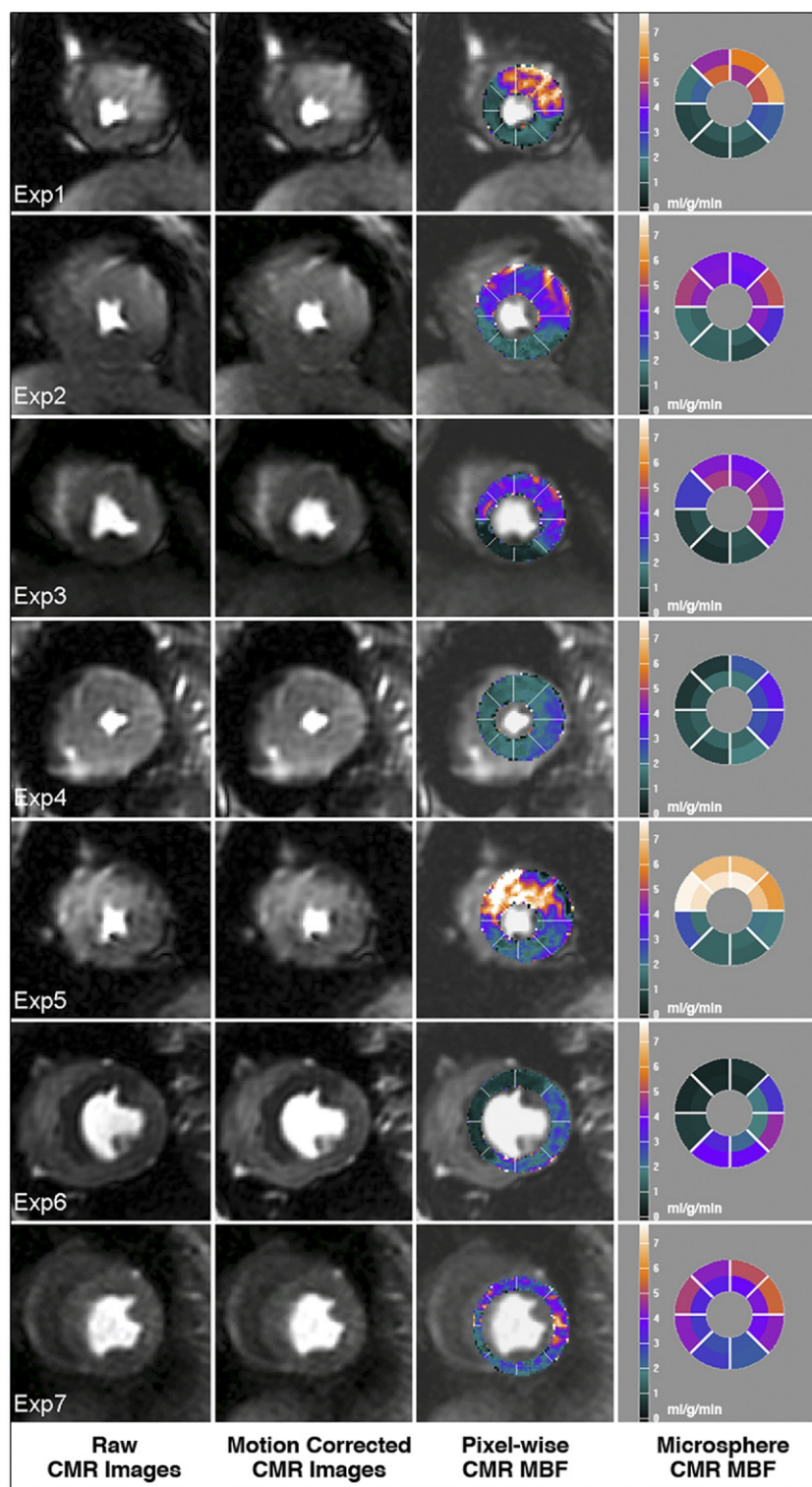
Figure 3. Qualitative Comparison of MBF by Pixel-Wise CMR and Microspheres

Cardiac magnetic resonance (CMR) perfusion pixel maps showing myocardial blood flow (MBF) estimates were in a similar range with microsphere absolute MBF (ml/min/g). Columns, from **left** to **right**: a raw image during early contrast enhancement, the result of non-rigid motion correction, the result of pixel-wise CMR MBF estimates, and reference microsphere absolute MBF.
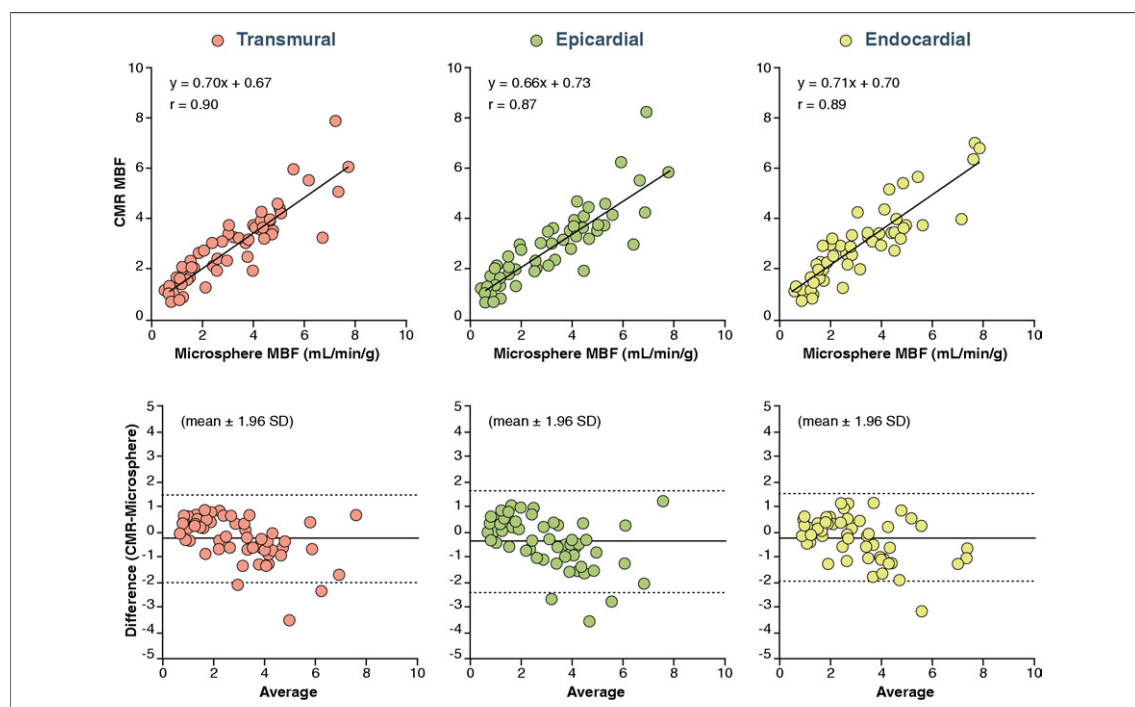
Figure 4. Comparison of MBF by Pixel-Wise CMR and Microspheres

Pixel-wise cardiac magnetic resonance (CMR) perfusion myocardial blood flow (MBF) estimates correlated well with microsphere absolute MBF measurements but showed minor underestimation of MBF.
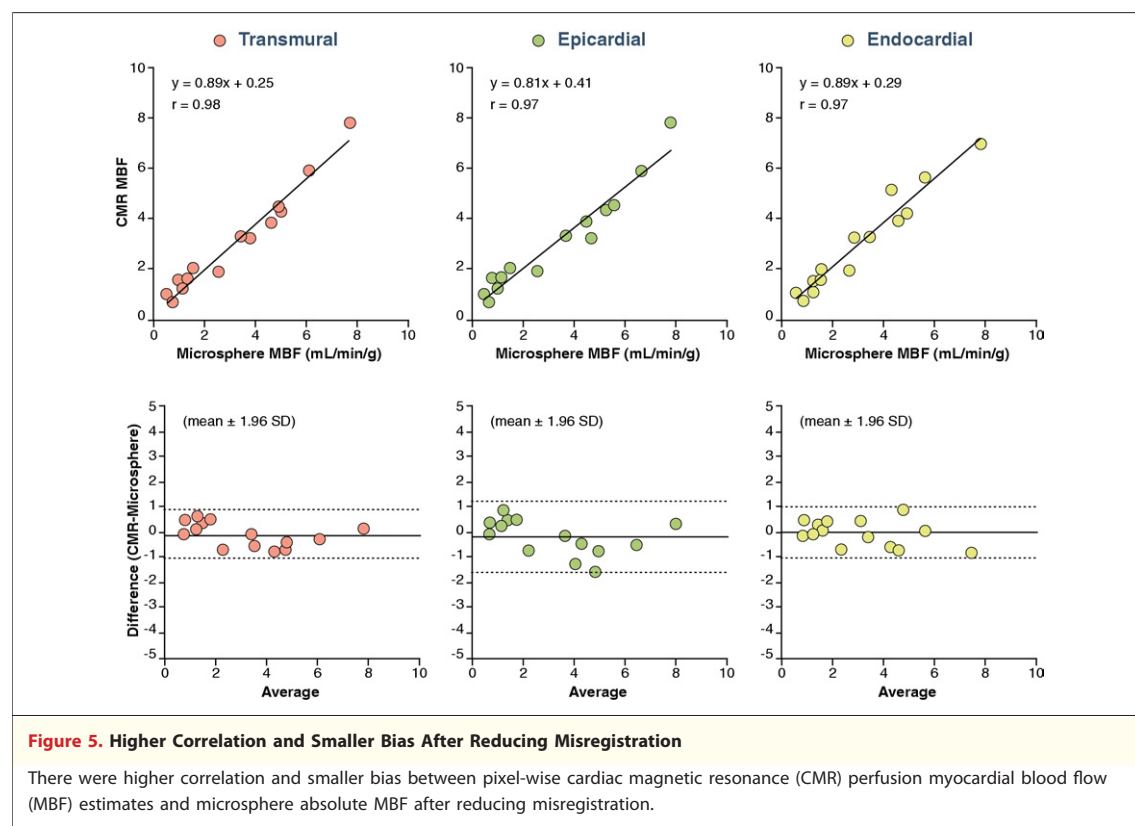
To study the heterogeneity of pixel-wise CMR perfusion MBF in hyperemic and remote regions, the CV of pixel-wise MBF in transmural, endocardial, and epicardial sectors was measured (Table 2). There was less variability of pixel-wise MBF estimates in hyperemic sectors compared with the remote. This smaller variability was consistent in transmural, endocardial, and epicardial sectors.

Because the selective coronary infusion of adenosine did not create transmural perfusion gradients in the dogs, we analyzed transmural perfusion gradients in patients with significant coronary artery stenosis as determined by invasive coronary angiography. Figure 7 shows examples of pixel-wise MBF maps for human first-pass perfusion CMR imaging at rest and during stress. Pixel-wise perfusion maps of the healthy volunteer (Patient #1) show MBF estimates in the range of 0.5 to 1.0 ml/g/min at rest, and increase to above 2.5 ml/g/min range during stress for all 3 coronary territories.

For 2 patients with single-vessel LAD disease (Patients #2 and #3), pixel-wise MBF maps of stress CMR showed transmural perfusion gradients in the LAD territory. In Patient #4, stress CMR maps showed a severe LAD perfusion defect corresponding to a 70% ostial stenosis and less severe subendocardial perfusion defects corresponding to

intermediate stenoses in the right coronary and circumflex coronary arteries. In Patient #5, there were obvious stress-induced perfusion defects in the LAD (80% stenosis) and right coronary artery territory (collateral-dependent occluded vessel), and a mild subendocardial perfusion defect associated with a terminal obtuse marginal branch with a 70% stenosis. There was reduced MBF in all myocardial regions on the stress CMR perfusion map of another patient with 3-vessel disease (Patient #6). Overall, CMR perfusion maps were more homogeneous at rest compared with stress CMR maps in all patients with CAD.

To quantify transmural gradient in patients with significant coronary stenosis, endocardial MBF, epicardial MBF, and endocardial-to-epicardial MBF ratio of the ischemic and remote regions in CMR perfusion pixel maps were compared. Table 3 shows there were no differential blood flows between endocardial to epicardial subsectors in the remote regions ($p = NS$). However, there were significant blood flow differences between endocardial and epicardial subsectors in the ischemic territories ($p < 0.001$). Both endocardial and epicardial MBF estimates in the ischemic regions were also significantly lower than in the remote regions ($p < 0.001$ for endocardial and $p < 0.01$ for epicardial comparisons).

Figure 5. Higher Correlation and Smaller Bias After Reducing Misregistration

There were higher correlation and smaller bias between pixel-wise cardiac magnetic resonance (CMR) perfusion myocardial blood flow (MBF) estimates and microsphere absolute MBF after reducing misregistration.

DISCUSSION

The importance of this paper is that it resolves the concept that perfusion information encoded in the first-pass CMR images is quantifiable at a pixel level (around 32 μl of tissue per pixel) in a canine model. We present an approach to generate comprehensive pixel-wise MBF maps for high-resolution quantitative visualization of first-pass gadolinium-enhanced perfusion CMR images. Both pixel-wise and sector-wise comparisons showed MBF estimates from CMR closely correlated with absolute microsphere measurements over a wide range of MBF values, particularly in analyses done in ways to minimize misregistration. The results of pixel-wise perfusion maps displayed on a calibrated color scale are qualitatively comparable to microsphere bull's-eye plots when displayed on the same absolute MBF color scale but at 15 times higher resolution. Although the animal model did not create statistically significant transmural perfusion gradients, such transmural perfusion gradients were present qualitatively and quantitatively on stress CMR perfusion maps in patients with significant coronary artery stenoses.

Theoretically and empirically, CMR imaging has sufficient spatial resolution to differentiate perfusion

between subendocardial and subepicardial regions (26). Transmural gradients of myocardial perfusion from CMR images have been compared in animal models (16,27), in normal volunteers (28), and in patients (29). These studies used a sector-by-sector approach and showed transmural flow differences in CMR perfusion. Pixel-wise semiquantitative perfusion maps can identify patients with CAD (5,8,30) but lack consistent scales for differentiating normal from abnormal. Pixel-wise fully quantitative perfusion maps have also been evaluated in normal animal models using intravascular contrast (31) and in normal human subjects (32). Although these studies have shown global perfusion differences between resting and hyperemic myocardium, regional perfusion changes have not previously been demonstrated at a pixel level.

Flow heterogeneity of myocardial perfusion. Flow heterogeneity within the heart is well documented in pre-clinical models (33) and represents an interplay among the heterogeneity of metabolism/physiology of the myocardium (34), coronary vascular anatomy at a small scale, and technical limitations related to perfusion methods such as microspheres (35). Bassingthwaighte et al. (36) showed that microspheres tend to systematically overestimate regions of high flow and
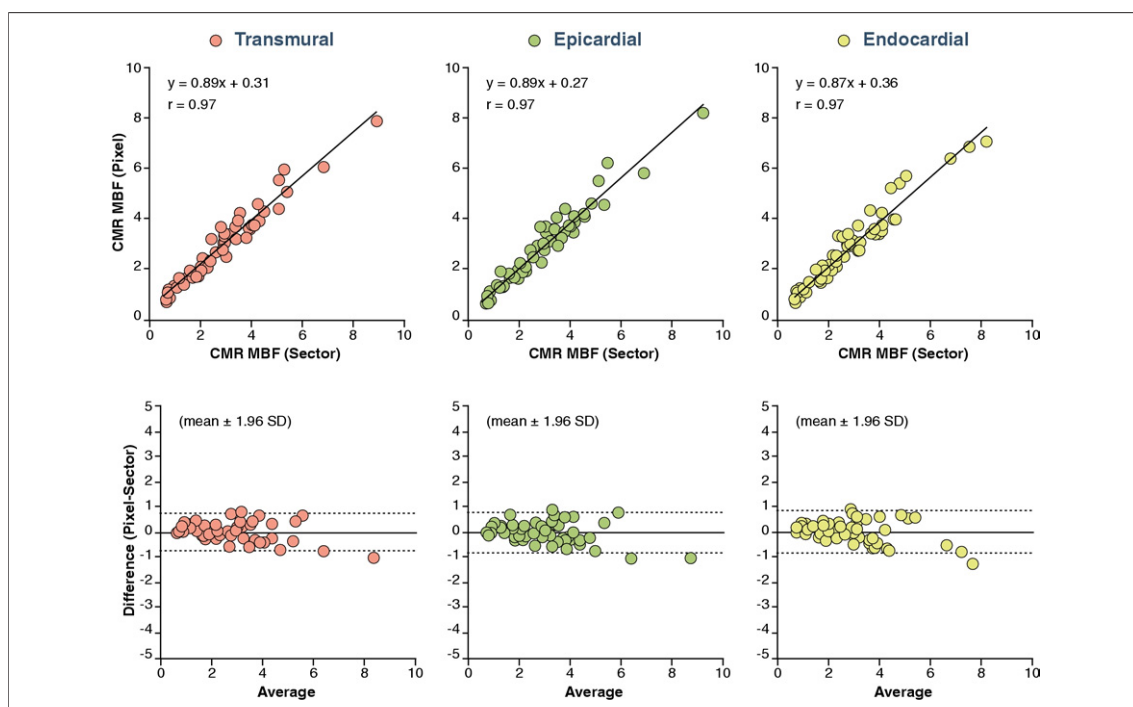
Figure 6. Comparison of MBF by Pixel-Wise and Sector-Wise CMR

Correlations between cardiac magnetic resonance (CMR) myocardial blood flow (MBF) estimated from pixel-wise and sector-wise time-signal intensity curves were excellent. Bland-Altman analysis showed there is no significant bias. MBF quantified at the pixel level does not intrinsically degrade the perfusion information content of the CMR images as estimated from sector-wise analysis.

underestimate regions of low flow, yet are sufficient for estimating regional flow in the heart. The current pixel-wise CMR MBF results (Table 2) have comparable or less variability than prior microsphere flow measurements with respect to absolute rest flow, vasodilated flow, and flow heterogeneity (33,37). With regard to flow heterogeneity versus sample size, the CMR pixel-wise perfusion estimates are less variable than predicted by the fractal model derived from the microspheres for such small tissue masses (37).

Compensating for nonrigid motion. Image registration is an essential image processing step for quan-

tifying CMR perfusion images at a pixel level. Motion artifacts are inevitable. Rigid-body image registration (38–44) has been studied, but these methods do not correct for local deformations. Some techniques compensate for nonrigid image motion semiautomatically (45) or automatically (46). In this study, we implemented a semiautomated, nonrigid image registration method, and this method performed well on all datasets.

Compensating for interstitial loading. CMR gadolinium contrast agents are imperfect perfusion tracers because they rapidly enter the extracellular space. Although the first-pass myocardial time-signal intensity is heavily perfusion dependent, interstitial loading of contrast can distort the measured time-signal intensity curves from what would be expected for an intravascular agent. Practically, the early phase of the myocardial time-signal intensity curves is

Table 1. Analysis of Endocardial MBF, Epicardial MBF, and Endocardial-to-Epicardial Ratio in Dogs CMR Perfusion Pixel Maps and Microspheres Measurements

Method	Endocardial	Epicardial	Ratio
CMR			
Hyperemic	4.64 ± 1.31	4.55 ± 1.08	1.05 ± 0.15
Remote	1.43 ± 0.48	1.44 ± 0.50	0.99 ± 0.19
Microspheres			
Hyperemic	4.53 ± 1.62	5.11 ± 0.38	0.88 ± 0.14
Remote	1.47 ± 0.64	1.32 ± 0.74	1.16 ± 0.17

Values are mean ± SD.
CMR = cardiac magnetic resonance; MBF = myocardial blood flow.

Table 2. The Variability of Pixel-Wise CMR MBF in Hyperemic and Remote Sectors as Represented by CV

CMR	Endocardial	Epicardial	Transmural
Hyperemic	0.15	0.18	0.19
Remote	0.19	0.23	0.22

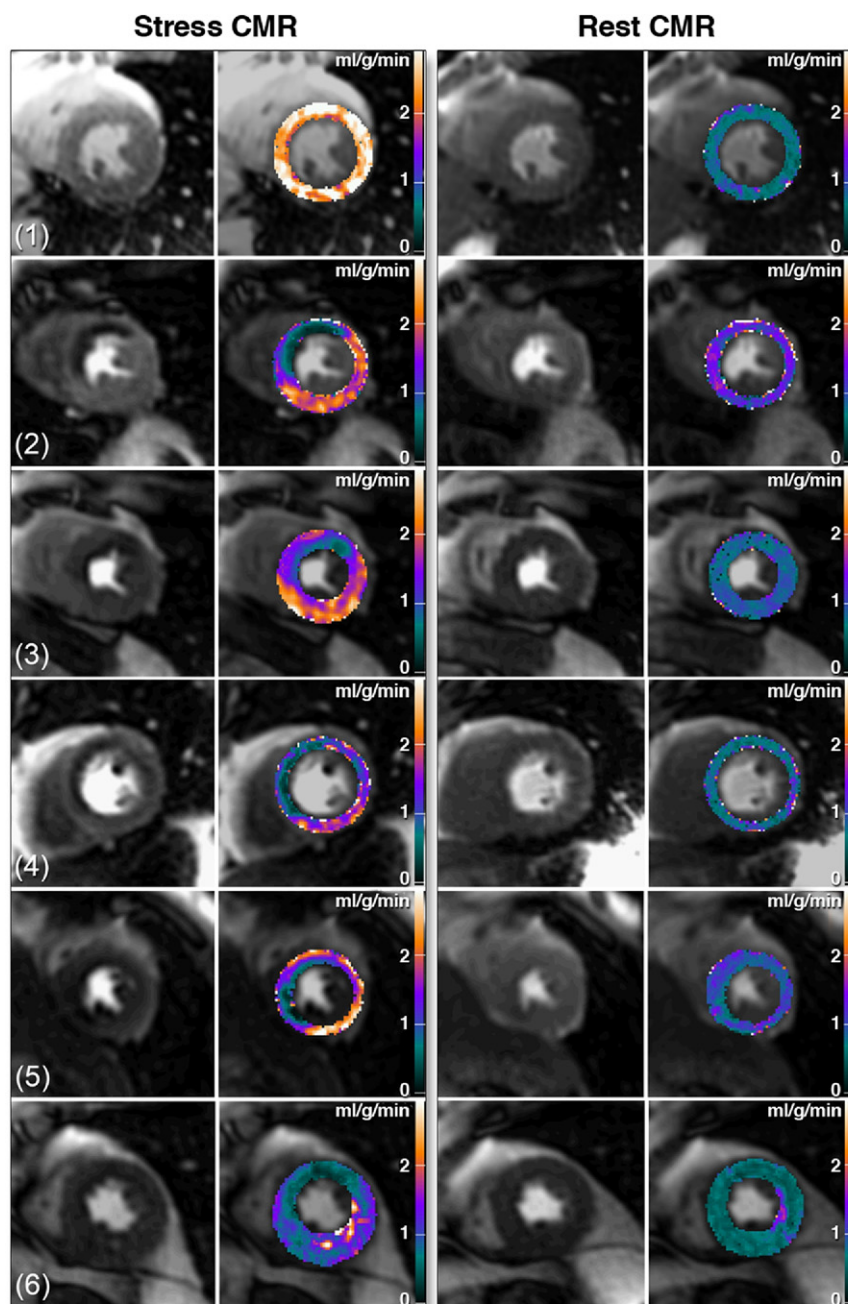CV = coefficient of variation; other abbreviations as in Table 1.

Figure 7. Clinical CMR Perfusion Pixel Maps

Pixel-wise cardiac magnetic resonance (CMR myocardial perfusion maps of a healthy volunteer [Patient #1] and patients with various degrees of coronary artery disease [Patients #2 to #6]). See the Results section for details and quantitative analysis.

less sensitive to the capillary leakage of contrast agent compared with the later portion of the curves (27). However, the interstitial loading during the later phase of contrast enhancement results in a large plateau in the myocardium several times higher than expected for the second pass of contrast.

Although the Fermi function approximates the shape of the impulse response of an intravascular tracer (25), it does not account for interstitial loading of the gadolinium contrast. As a result, Fermi function–constrained deconvolution should be limited to the first myocardial contrast passage

Table 3. Analysis of Endocardial MBF, Epicardial MBF, and Endocardial-to-Epicardial Ratio CMR Perfusion Pixel Maps in Patients

CMR	Endocardial	Epicardial	Ratio
Ischemic	0.76 ± 0.38	1.31 ± 0.45	0.58 ± 0.22
Remote	2.03 ± 0.30	2.05 ± 0.58	1.03 ± 0.20

Values are mean ± SD.
Abbreviations as in Table 1.

(15,24). The proposed impulse response function compensates for these problems by incorporating an offset term into the deconvolution model to allow the time intensity curve fitting beyond the first pass of the contrast. This approach can reduce the subjectivity of selecting the first-pass range in CMR perfusion quantification and facilitate automating perfusion quantification.

Nonlinear signal intensity in CMR perfusion imaging. The nonlinearity between myocardial signal intensity and gadolinium contrast concentration might affect MBF quantification (47). The current study used dual-bolus contrast administration (12) and a half-dose contrast with fast imaging with steady-state precession sequence parameters to improve the linearity of CMR signal intensity and to minimize the need for nonlinear signal intensity calibration.

Clinical implications. Quantitative and objective analyses of CMR perfusion images have the potential to improve clinical diagnosis. Objective semi-quantitative methods have become important clinical tools in single-photon emission computed tomography myocardial perfusion imaging (48,49). Quantitative measurements of myocardial perfusion may have a similar impact in CMR imaging. Examples of pixel-wise CMR perfusion maps as presented in this study show transmural perfusion gradients can be differentiated in patients with various degrees of ischemia. Thus, first-pass CMR perfusion imaging provides sufficient spatial resolution to estimate MBF at the pixel level, which may someday improve the diagnosis of CAD in patients.

Study limitations. The reference standard microsphere MBF has a resolution about 15 times lower than pixel-wise CMR MBF estimates. This difference in spatial resolution limits the direct comparison of MBF between CMR and microspheres to the sector level. However, internal comparisons of pixel-wise and sector-wise CMR MBF estimates are consistent and do not appear limited by the pixel-wise signal-to-noise ratio.

Misregistration between the CMR imaging slice versus pathological microsphere slice is always a potential source of errors. Minimizing the probability of misregistration improves the correlations between CMR and microspheres estimates of MBF, as shown in the Figure 4 and Figure 5 comparisons.

The current study used manual tracing of myocardial borders for nonrigid image registration. Although the method is effective, it is time consuming. Automated nonrigid image registration (46) may compensate for motion artifacts and may improve the workflow of pixel-wise CMR perfusion quantification.

The number of animals used in this study was limited, and the animal model chosen did not include different levels of coronary stenoses or complete occlusion, which may limit the accuracy of pixel-wise MBF estimates under total ischemic conditions. The sample size of clinical studies was also limited, although various degrees of ischemia were incorporated to demonstrate that pixel-wise CMR perfusion maps can detect transmural perfusion gradients or differential blood flow from single- or multiple-vessel stenoses. Further trials are required to evaluate whether pixel-wise CMR perfusion quantification may improve the diagnostic accuracy for detecting CAD compared to conventional sector-based approach.

CONCLUSIONS

MBF in gadolinium-enhanced first-pass CMR perfusion imaging can be quantified at a pixel level that is equivalent to 32 μl per sample in this canine model. The heterogeneity of pixel-wise CMR MBF estimates is comparable or smaller than previously published microsphere results in canines. High-resolution pixel-wise CMR perfusion maps can detect transmural perfusion gradients and may someday improve the objectivity of diagnosing CAD in patients.

REFERENCES

1. Al-Saadi N, Nagel E, Gross M, et al. Noninvasive detection of myocardial ischemia from perfusion reserve based on cardiovascular magnetic resonance. Circulation 2000; 101:1379–83.

2. Giang TH, Nanz D, Coulden R, et al. Detection of coronary artery disease by magnetic resonance myocardial perfusion imaging with various contrast medium doses: first European multi-centre experience. Eur Heart J 2004;25:1657–65.

3. Nagel E, Klein C, Paetsch I, et al. Magnetic resonance perfusion measurements for the noninvasive detection of coronary artery disease. Circulation 2003;108:432–7.

4. Paetsch I, Jahnke C, Wahl A, et al. Comparison of dobutamine stress magnetic resonance, adenosine stress magnetic resonance, and adenosine stress magnetic resonance perfusion. Circulation 2004;110:835–42.

5. Panting JR, Gatehouse PD, Yang GZ, et al. Echo-planar magnetic resonance myocardial perfusion imaging: parametric map analysis and comparison with thallium SPECT. J Magn Reson Imaging 2001;13:192–200.

6. Schwitter J, Nanz D, Kneifel S, et al. Assessment of myocardial perfusion in coronary artery disease by magnetic resonance: a comparison with positron emission tomography and coronary angiography. Circulation 2001;103:2230–5.

7. Plein S, Radjenovic A, Ridgway JP, et al. Coronary artery disease: myocardial perfusion MR imaging with sensitivity encoding versus conventional angiography. Radiology 2005;235:423–30.

8. Thiele H, Plein S, Breeuwer M, et al. Color-encoded semiautomatic analysis of multi-slice first-pass magnetic resonance perfusion: comparison to tetrofosmin single photon emission computed tomography perfusion and X-ray angiography. Int J Cardiovasc Imaging 2004;20:371–84.

9. Bunce NH, Reyes E, Keegan J, et al. Combined coronary and perfusion cardiovascular magnetic resonance for the assessment of coronary artery stenosis. J Cardiovasc Magn Reson 2004; 6:527–39.

10. Doyle M, Fuisz A, Kortright E, et al. The impact of myocardial flow reserve on the detection of coronary artery disease by perfusion Imaging methods: an NHLBI WISE study. J Cardiovasc Magn Reson 2003;5:475–85.

11. Ibrahim T, Nekolla SG, Schreiber K, et al. Assessment of coronary flow reserve: comparison between contrast-enhanced magnetic resonance imaging and positron emission tomography. J Am Coll Cardiol 2002;39:864–70.

12. Christian TF, Rettmann DW, Aletras AH, et al. Absolute myocardial perfusion in canines measured by using dual-bolus first-pass MR imaging. Radiology 2004;232:677–84.

13. Hsu LY, Rhoads KL, Holly JE, Kellman P, Aletras AH, Arai AE. Quantitative myocardial perfusion analysis with a dual-bolus contrast-enhanced first-pass MRI technique in humans. J Magn Reson Imaging 2006;23:315–22.

14. Jerosch-Herold M, Swingen C, Seethamraju RT. Myocardial blood flow quantification with MRI by model-independent deconvolution. Med Physics 2002;29:886–97.

15. Jerosch-Herold M, Wilke N, Stillman AE, Wilson RF. Magnetic resonance quantification of the myocardial perfusion reserve with a Fermi function model for constrained deconvolution. Med Physics 1998;25:73–84.

16. Lee DC, Simonetti OP, Harris KR, et al. Magnetic resonance versus radionuclide pharmacological stress perfusion imaging for flow-limiting stenoses of varying severity. Circulation 2004;110:58–65.

17. Klocke FJ, Simonetti OP, Judd RM, et al. Limits of detection of regional differences in vasodilated flow in viable myocardium by first-pass magnetic resonance perfusion imaging. Circulation 2001;104:2412–6.

18. Christian TF, Aletras AH, Arai AE. Estimation of absolute myocardial blood flow during first-pass MR perfusion imaging using a dual-bolus injection technique: comparison to single-bolus injection method. J Magn Reson Imaging 2008;27:1271–7.

19. Schreiber WG, Schmitt M, Kalden P, Mohrs OK, Kreitner KF, Thelen M. Dynamic contrast-enhanced myocardial perfusion imaging using saturation-prepared TrueFISP. J Magn Reson Imaging 2002;16:641–52.

20. Gatehouse PD, Elkington AG, Ablitt NA, Yang GZ, Pennell DJ, Firmin DN. Accurate assessment of the arterial input function during high-dose myocardial perfusion cardiovascular magnetic resonance. J Magn Reson Imaging 2004;20:39–45.

21. Hsu L-Y, Aletras AH, Arai AE. Correcting surface coil intensity inhomogeneity improves quantitative analysis of cardiac magnetic reso-

nance images. Paper presented at: Biomedical Imaging: From Nano to Macro, 2008. ISBI 2008. 5th IEEE International Symposium; May 14-17, 2008; Paris, France.

22. Zierler KL. Theoretical basis of indicator-dilution methods for measuring flow and volume. Circ Res 1962;10:393–407.

23. Zierler KL. Equations for measuring blood flow by external monitoring of radioisotopes. Circ Res 1965;16:309–21.

24. Jerosch-Herold M, Seethamraju RT, Swingen CM, Wilke NM, Stillman AE. Analysis of myocardial perfusion MRI. J Magn Reson Imaging 2004; 19:758–70.

25. Axel L. Tissue mean transit-time from dynamic computed-tomography by a simple deconvolution technique. Invest Radiol 1983;18:94–9.

26. Wilke NM, Jerosch-Herold M, Zenovich A, Stillman AE. Magnetic resonance first-pass myocardial perfusion imaging: clinical validation and future applications. J Magn Reson Imaging 1999;10:676–85.

27. Jerosch-Herold M, Wilke N, Wang Y, et al. Direct comparison of an intravascular and an extracellular contrast agent for quantification of myocardial perfusion. Int J Card Imaging 1999;15:453–464.

28. Muehling OM, Jerosch-Herold M, Panse P, et al. Regional heterogeneity of myocardial perfusion in healthy human myocardium: assessment with magnetic resonance perfusion imaging. J Cardiovasc Magn Reson 2004; 6:499–507.

29. Muehling OM, Wilke NM, Panse P, et al. Reduced myocardial perfusion reserve and transmural perfusion gradient in heart transplant arteriopathy assessed by magnetic resonance imaging. J Am Coll Cardiol 2003;42:1054–60.

30. Su MYM, Yang KC, Wu CC, et al. First-pass myocardial perfusion cardiovascular magnetic resonance at 3 Tesla. J Cardiovasc Magn Reson 2007;9:633–44.

31. Goldstein TA, Jerosch-Herold M, Misselwitz B, Zhang H, Gropler RJ, Zheng J. Fast mapping of myocardial blood flow with MR first-pass perfusion imaging. Magn Reson Med 2008;59:1394–400.

32. Pack NA, DiBella EVR, Rust TC, et al. Estimating myocardial perfusion from dynamic contrast-enhanced CMR with a model-independent deconvolution method. J Cardiovasc Magn Reson 2008;10:52.

33. Austin RE Jr., Aldea GS, Coggins DL, Flynn AE, Hoffman JI. Profound spatial heterogeneity of coronary reserve. Discordance between patterns of resting and maximal myocardial blood flow. Circ Res 1990;67:319–31.

34. Decking UK. Spatial heterogeneity in the heart: recent insights and open questions. News Physiol Sci 2002;17: 246–50.

35. Decking UK, Pai VM, Bennett E, et al. High-resolution imaging reveals a limit in spatial resolution of blood flow measurements by microspheres. Am J Physiol Heart Circ Physiol 2004;287:H1132–40.

36. Bassingthwaighte JB, Malone MA, Moffett TC, et al. Molecular and particulate depositions for regional myocardial flows in sheep. Circ Res 1990; 66:1328–44.

37. Bassingthwaighte JB, King RB, Roger SA. Fractal nature of regional myocardial blood flow heterogeneity. Circ Res 1989;65:578–90.

38. Dornier C, Ivancevic MK, Thevenaz P, Vallee JP. Improvement in the quantification of myocardial perfusion using an automatic spline-based registration algorithm. J Magn Reson Imaging 2003;18:160–8.

39. Bidaut LM, Vallee JP. Automated registration of dynamic MR images for the quantification of myocardial perfusion. J Magn Reson Imaging 2001;13:648–55.

40. Gupta SN, Solaiyappan M, Beache GM, Arai AE, Foo TKF. Fast method for correcting image misregistration due to organ motion in timeseries MRI data. Magn Reson Med 2003;49:506–14.

41. Wong KK, Yang ES, Wu EX, Tse HF, Wong ST. First-pass myocardial perfusion image registration by maximization of normalized mutual information. J Magn Reson Imaging 2008; 27:529–37.

42. Milles J, van der Geest RJ, Jerosch-Herold M, Reiber JH, Lelieveldt BP. Fully automated motion correction in first-pass myocardial perfusion MR image sequences. IEEE Trans Med Imaging 2008;27:1611–21.

43. Delzescaux T, Frouin F, de Cesare A, et al. Using an adaptive semiautomated self-evaluated registration technique to analyze MRI data for myocardial perfusion assessment. J Magn Reson Imaging 2003;18:681–90.

44. Comte A, Lalande A, Aho S, Walker PM, Brunotte F. Realignment of myocardial first-pass MR perfusion images using an automatic detection of the heart-lung interface. Magn Reson Imaging 2004;22: 1001–9.

45. Yang GZ, Burger P, Panting J, et al. Motion and deformation tracking for short-axis echo-planar myocardial perfusion imaging. Med Image Anal 1998;2:285–302.

46. Xue H, Zuehlsdorff S, Kellman P, et al. Unsupervised inline analysis of cardiac perfusion MRI. Med Image Comput Comput Assist Interv 2009; 12:741–9.

47. Hsu LY, Kellman P, Arai AE. Nonlinear myocardial signal intensity correction improves quantification of contrast-enhanced first-pass MR perfusion in humans. J Magn Reson Imaging 2008;27:793–801.

48. Germano G, Kavanagh PB, Slomka PJ, Van Kriekinge SD, Pollard G, Berman DS. Quantitation in gated perfusion SPECT imaging: the Cedars-Sinai approach. J Nucl Cardiol 2007;14:433–54.

49. Slomka PJ, Nishina H, Abidov A, et al. Combined quantitative supine-prone myocardial perfusion SPECT improves detection of coronary artery disease and normalcy rates in women. J Nucl Cardiol 2007;14:44–52.